Effects of Inherent Fabric Anisotropy and Intermediate Principal Stress on Constitutive Behavior of Uncemented and Cemented Sands

Mojtaba Rahimi*, Dave Chan, Alireza Nouri, Rouzbeh Rasouli

Department of Civil & Environmental Engineering, University of Alberta, Edmonton, AB, Canada.

* Corresponding author: rahimi2726@gmail.com & rahimi2726@yahoo.com

Keywords: Constitutive model, uncemented and cemented sands, undrained and drained hollow cylinder tests, inherent anisotropy, monotonic and cyclic loading.

Abstract

Sand response changes with intensity of cementation bonds between sand grains, magnitude of intermediate principal stress and with fabric anisotropy. First a critical state bounding surface plasticity model is presented in this paper. In this constitutive model, the loading surface always passes through the current stress state regardless of location or position of the stress path. Second to simulate hollow cylinder tests which represent different modes of shearing including triaxial compression and triaxial extension, the fabric anisotropy and $\boldsymbol{b}$-parameter are incorporated in the model. Simultaneous integration of cohesion, non-associated flow rule, fabric anisotropy, kinematic hardening, critical state and state parameter makes the proposed model unique compared to previous proposed bounding surface models. Comparison of model outcomes and hollow cylinder experimental tests shows great predictive capability of the proposed model. Sensitivity analysis also suggests that triaxial compression and triaxial extension are respectively strongest and weakest modes of shearing.

1. Introduction

The structure in natural soils is a combination of bonding and fabric. Therefore the overall behavior of cemented sand depends not only on the degree of cementation between sand particles, but also on fabric in sand. Fabric reflects particle orientation, and particle contact arrangements. It describes the geometrical arrangement/packing of particles in general [1, 2]. During deposition process under

earth gravity, sand particles usually deposit anisotropically and form fabric structure with cross-anisotropy (or transverse-isotropy). Cross-anisotropy as an inherent anisotropy is featured by one direction with distinctive anisotropy perpendicular to a bedding planes where it is almost isotropic. The perpendicular direction is the direction of deposition and is referred to as the axis of anisotropy [3]. Similar to uncemented sand, fabric is expected to affect cemented sand behavior namely its stiffness, strength and dilatancy (the contractive or dilative tendency upon shearing) [2, 3]. Most constitutive models, however, are not formulated with considering the effect of bonding and fabric anisotropy simultaneously [3, 4, 5]. That is, some constitutive models capture the influence of void ratio/mean stress on sand behavior, but neglect the effect of fabric. However, there is little doubt that sand fabric is an influential parameter in the constitutive behavior of sand [4].

Investigations at the microscopic level have shown that orientation of sand particles changes slightly even after large shear deformation. In other words, the inherent (structural/intrinsic) fabric anisotropy may be assumed constant during shearing process [6].

Soil fabric is incorporated in the proposed model using a symmetric fabric tensor F_{ij} which is kept constant to account for material inherent anisotropy and a scalar-valued state variable A which can represent the material anisotropic state.

2. A critical state bounding surface constitutive model for sand and cemented sand

The main components of the proposed constitutive model are elasticity, loading surface and bounding surface, flow rule, and normalized plastic modulus. They are concisely discussed here.

2.1 Elasticity

The elastic moduli (i.e. shear and bulk elastic modulus) are defined as follows:

$$G = G_a \frac{(2.973 - e)^2}{1 + e} \left(\frac{p}{p_{atm}} \left(1 + \sqrt{\frac{p_o}{p}} \right) \right)^n \quad (1)$$

$$K = K_a \frac{(2.973 - e)^2}{1 + e} \left(\frac{p}{p_{atm}} \left(1 + \sqrt{\frac{p_o}{p}} \right) \right)^n \quad (2)$$

where G and K are elastic shear modulus and bulk modulus, respectively, e is void ratio, G_a and K_a are reference elastic moduli associated with p_{atm} which is the atmospheric pressure, p is the mean effective stress, and p_o is an additional strength which comes from the material cementation. A value of 0.5-0.55 is usually allocated for n, depending on the type of sand.

The elastic moduli are defined for unloading conditions as follows:

$$G = |\eta| \, G_a \frac{(2.973 - e)^2}{1 + e} \left(\frac{p}{p_{atm}} \left(1 + \sqrt{\frac{p_o}{p}} \right) \right)^n \quad (3)$$

$$K = |\eta| \, K_a \frac{(2.973 - e)^2}{1 + e} \left(\frac{p}{p_{atm}} \left(1 + \sqrt{\frac{p_o}{p}} \right) \right)^n \quad (4)$$

where $|\eta|$ denotes the absolute value of the stress ratio. Incorporation of η in the definition of the elastic moduli results in the prediction of a stiffer response at the start of unloading and then a softer response with progress of unloading. Suggestion of these expressions for the unloading elastic moduli comes from experimental observations which shows a sudden increase in stiffness immediately after the inception of unloading accompanied with a slow decrease in its magnitude when soil experiences progressive unloading [7].

2.2 loading surface and bounding surface

The loading surface (f) and bounding surface (F) in terms of the conventional triaxial parameters are defined as (Fig. 1):

$$f = \left(\frac{q - q_a}{p - p_a + p_t} - \alpha\right)^2 - M_\alpha^2\left(1 - \sqrt{\frac{p - p_a + p_t}{p_b}}\right) = 0 \quad (5)$$

$$F = \left(\frac{\bar{q} - \bar{q}_a}{\bar{p} - \bar{p}_a + p_t} - \alpha\right)^2 - M_\alpha^2\left(1 - \sqrt{\frac{\bar{p} - \bar{p}_a + p_t}{\bar{p}_b}}\right) = 0 \quad (6)$$

$$M_\alpha^2 = (5M_p - \alpha)(M_p - \alpha) \quad (7)$$

where q is the deviator stress, and p_a and q_a are components of the kinematic hardening tensor, M_p is the stress ratio at the peak of the undrained effective stress path (UESP), α is a scalar whose magnitude is zero for isotropically consolidated sands, p_t is tensile strength, and p_b is hardening parameter for the loading surface. The kinematic hardening tensor is assumed to lie initially at the origin of the stress space, implying for the first time loading: $(p_a, q_a) = (0,0)$.

The superimposed bar indicates the bounding surface variables.

To ensure that the loading surface will not cross the bounding surface, it is assumed that the initial ratio of size of the two surfaces remain constant during the shearing process. It is also presumed that the kinematic hardening components always coincide for the two surfaces, i.e. $(p_a, q_a) = (\bar{p}_a, \bar{q}_a)$.

The additional strength p_o and tensile strength p_t are assumed to be linked together using the following relationship:

$$p_t = \beta p_o \quad (8)$$

where β is a model parameter.

It is also assumed that p_o decreases with plastic deformation due to destruction of sand structure by the following law:

$$dp_o = -\gamma p_o d\left|\varepsilon_q^p\right| \quad (9)$$

where γ is a model parameter which determines the rate of bond degradation, and dp_o indicates change in p_o due to change in plastic deviator strain.

Armstrong and Frederick's kinematic hardening law [8] is chosen to control the evolution of the loading surface and bounding surface as follows:

$$\dot{p}_\alpha = \frac{2}{3} c_1 \frac{\dot{\varepsilon}_p^p}{3} - c_2 p_\alpha \dot{z} \quad (10)$$

$$\dot{q}_\alpha = c_1 \, \dot{\varepsilon}_q^p - c_2 \, q_\alpha \, \dot{z} \tag{11}$$

where c_1 and c_2 are model constants, $\dot{\varepsilon}_q^p$ and $\dot{\varepsilon}_p^p$ are plastic deviator and volumetric strain increments, respectively, and $\dot{z}$ is the accumulative plastic strain increment which is expressed as:

$$\dot{z} = \sqrt{\frac{2}{3} \dot{\varepsilon}_{ij}^p \, \dot{\varepsilon}_{ij}^p} \tag{12}$$

where $\dot{\varepsilon}_{ij}^p$ denotes components of plastic strain increment tensor.

p_α and q_α are defined as:

$$p_\alpha = \frac{\alpha_{11} + 2\alpha_{33}}{3} \tag{13}$$

$$q_\alpha = \alpha_{11} - \alpha_{33} \tag{14}$$

M_p is calculated by the model for compression and extension as follows [9, 10]:

$$M_{p,c} = \frac{6sin\varphi_{p,c}}{3 - sin\varphi_{p,c}} \tag{15}$$

$$M_{p,e} = \frac{6sin\varphi_{p,e}}{3 + sin\varphi_{p,e}} \tag{16}$$

in which $\varphi_{p,c}$ and $\varphi_{p,e}$ are the friction angles at the current peak shear stress in the triaxial compression and triaxial extension tests, respectively. They can be calculated by:

$$\sin \varphi_{p,c} = sin\varphi_\mu - k_p \psi_p \tag{17}$$

$$\sin \varphi_{p,e} = sin\varphi_\mu - k_p \psi_p - a_p \tag{18}$$

where $\psi_p = e - e_p$ is the state parameter at the current peak in which e is void ratio, and e_p is the critical state void ratio which is calculated at mean effective stress corresponding to M_p, φ_μ is the interparticle friction angle and k_p and a_p are model parameters.

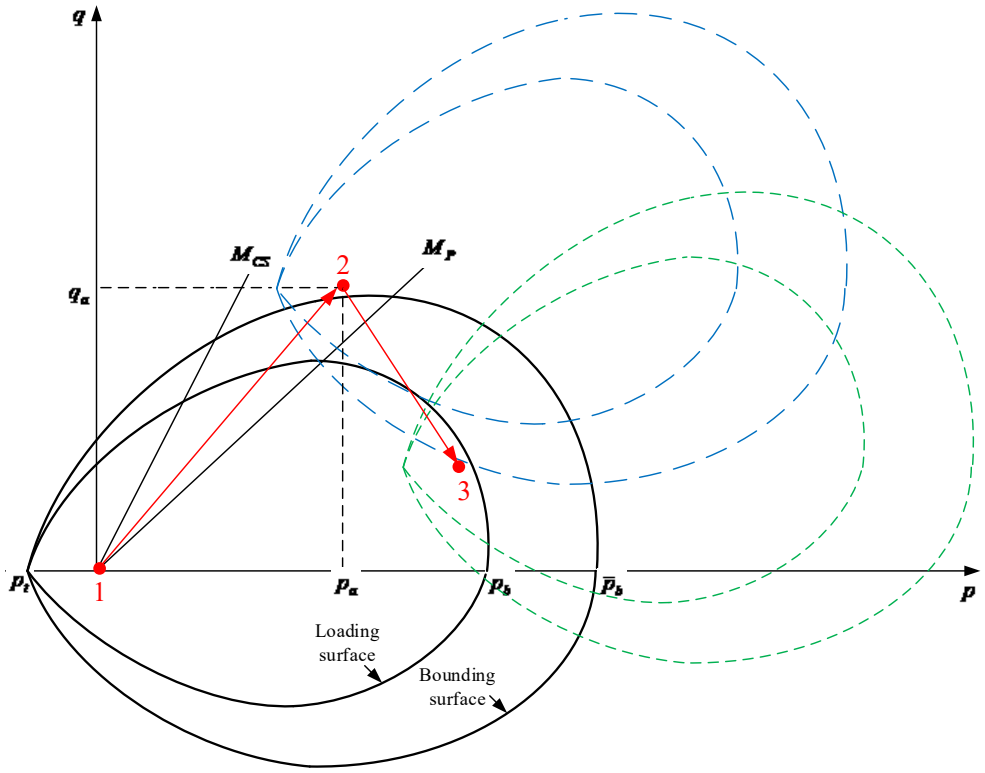

Fig. 1 Schematic representation of simultaneous movement of the loading and bounding surfaces during loading (path 1-2) and unloading (path 2-3).

2.3 Flow rule

The following non-associated flow rule is expressed similar to Yu et al. [11] as:

$$D = \sqrt{\frac{2}{3}}\left(A\left(M_{pt} - |\eta|\right) + \frac{6B}{C}\right) \tag{19}$$

$$A = \frac{9}{C} \tag{20}$$

$$C = 9 + 3M_{pt} - 2M_{pt}|\eta| + 4B \tag{21}$$

$$B = \frac{coh}{p}\sqrt{\left(2M_{pt} + 3\right)\left(-M_{pt} + 3\right)} \tag{22}$$

where D is dilatancy rate, coh is cohesion, and M_{pt} is the phase transformation stress ratio. Cohesion is assumed to diminish with the total plastic strain increment as:

$$dcoh = coh\, e^{-\xi\sqrt{(\dot{\varepsilon}_q^p)^2+(\dot{\varepsilon}_p^p)^2}} \tag{23}$$

where ξ determines rate of cohesion degradation.

M_{pt} is defined for compression and extension using the following relationships [9,10]:

$$M_{pt,c} = \frac{6sin\varphi_{pt,c}}{3 - sin\varphi_{pt,c}} \tag{24}$$

$$M_{pt,e} = \frac{6sin\varphi_{pt,e}}{3 + sin\varphi_{pt,e}} \tag{25}$$

where

$$sin\varphi_{PT,c} = sin\varphi_{cs} + k_{PT}\psi_s \tag{26}$$

$$sin\varphi_{PT,e} = sin\varphi_{cs} + k_{PT}\psi_s + a_{PT} \tag{27}$$

in which φ_{cs} is the critical state friction angle, $\psi_s = e - e_{cs}$ is the state parameter [4, 12], e_{cs} is the critical void ratio and k_{PT} and a_{PT} are both model parameters.

It is worthy to note that modelling the flow rule behavior of sand/cemented sand is difficult because the responses are not the same under loading and unloading conditions [13]. Moreover, sand behavior becomes even more complex due to inherent anisotropy. Rowe [14] and Roscoe et. al. [15] presented two various forms of flow rules for sand, which have been broadly used in elastoplastic models of sand [13]. Most of proposed stress-dilatancy models are based on Roscoe's or Rowe's flow rule, for example Nova [16], Jefferies [17], Manzari and Dafalias [18] and Gajo and Wood [19]. Few proposed stress-dilatancy models has considered the effect of fabric anisotropy. Wan and Guo's model [20] is among very few models that considered fabric in formulation of the stress-dilaancy [13]. Yin and Chang [13] modelled flow rule using a micro-mechanism approach in which slip mechanism was considered for the dilatancy response between two particles. Because of the differences in slip patterns for unloading and loading conditions, two different forms of the stress-dilatancy was proposed for loading and unloading conditions.

In the proposed model in this paper, the same flue rule is used for both loading and unloading conditions. Also fabric is not directly formulated in the flow rule.

2.4 Normalized plastic modulus

The normalized plastic modulus (H_n) is calculated using the following equations:

$$H_n = -\sqrt{\frac{2}{3}}\frac{1}{\left|\frac{\partial f}{\partial q}\right|}\frac{\partial f}{\partial p_b}\frac{\partial p_b}{\partial \varepsilon_q^p} + {H_n}^{kinematic} \tag{28}$$

$$\frac{\partial p_b}{\partial \varepsilon_q^p} = \frac{hG_{ini}}{\left(p_f - p_c\right)_{ini}}\left(p_f - p_c\right) - (1+\beta)\gamma p_o \tag{29}$$

$${H_n}^{kinematic} = R\left(\frac{2}{9}c_1 D - c_2\, p_\alpha \sqrt{\frac{2}{9}D^2 + 1}\right) + c_1 - c_2 u_Q q_\alpha \sqrt{\frac{2}{9}D^2 + 1} \tag{30}$$

$$R = \sqrt{\frac{2}{3}}\frac{\frac{\partial f}{\partial p}}{\frac{\partial f}{\partial q}} \tag{31}$$

$$u_Q = \frac{\frac{\partial f}{\partial q}}{\left|\frac{\partial f}{\partial q}\right|} \tag{32}$$

where

h is a material parameter, p_f is the failure mean effective stress, G_{ini} is the initial value of G at the start of shearing, and p_c is the effective preconsolidation stress. p_f is obtained using an iterative method such as Newton-Raphson from the following equation:

$$p_f = \frac{p - p_a}{\left(1 - \frac{(\frac{M_f p_f - q_a}{p_f - p_a} - \alpha)^2}{M_\alpha^2}\right)^2} \tag{33}$$

Calculation of M_f is based on $sin\varphi_f$ which itself is calculated by:

$$sin\varphi_f = sin\varphi_{cs} - k_f\psi_s \tag{34}$$

where k_f is a model parameter.

H_n for unloading, i.e. $H_{n,u}$, is assumed to be linked to that for loading as:

$$\frac{H_{n,u}}{H_n} = R_u\sqrt{\frac{p}{p_{atm}}|\eta|} \tag{35}$$

where R_u is a model constant.

3. Fabric tensor

The orientation of non-spherical particles in a sand deposit can be represented using a second order fabric tensor as follows [6]:

$$F_{ij} = \frac{1}{2N}\sum_{k=1}^{2N} n_i^k n_j^k \tag{36}$$

where N is number of particles in a representative volume, and n is unit vector along major axis of elongation of the particle.

The magnitude of components of F_{ij} represents the net portion of particles which are statistically oriented towards a specific direction. F_{ij} is clearly symmetric and thus, it can be represented by three principal values of F_1, F_2, and F_3 (not necessarily implying that $F_1 \geq F_2 \geq F_3$), and three corresponding principal directions. If we assume that the principal axes of the soil fabric coincide with a reference coordinate system (x_1', x_2', x_3'), where the $x_2' - x_3'$ plane defines the isotropic plane of the fabric (i.e. bedding plane), and the x_1' axis shows the direction of deposition (i.e. perpendicular to the bedding plane), the fabric tensor can be defined as [6]:

$$F_{ij}' = \begin{pmatrix} F_1 & 0 & 0 \\ 0 & F_2 & 0 \\ 0 & 0 & F_3 \end{pmatrix} \tag{37}$$

In which $F_2 = F_3$ due to transverse-isotropy. It can be shown that F_{ij} has a unit trace which implies that $F_1 = 1 - F_2 - F_3 = 1 - 2F_3$. Therefore for a transversely isotropic soil with a given deposition direction (usually in the vertical direction), only one scalar quantity is required to define the fabric tensor. Oda and

Nakayama [21] proposed the following symmetric second order fabric tensor [3,5,6]:

$$F'_{ij} = \frac{1}{3+\Delta}\begin{pmatrix} 1-\Delta & 0 & 0 \\ 0 & 1+\Delta & 0 \\ 0 & 0 & 1+\Delta \end{pmatrix} \tag{38}$$

where Δ is a scalar that characterizes the magnitude of the cross-anisotropy. Δ is a model parameter which ranges from zero in the case of complete isotropy ($F'_{ij} = I/3 = \delta_{ij}/3$) to unity in the case of maximum anisotropy when the major axis of all particles are distributed in $x'_2 - x'_3$ plane (i.e. when the fabric is strongest in the bedding plane). Thus the fabric tensor F'_{ij} characterizes both the intensity and orientation of the inherent material anisotropy for a specific sand deposit.

4. Anisotropic state variable

The introduction of fabric tensor into a constitutive model which includes other tensor variables such as the stress tensor requires special considerations. This may lead to complex mathematical relationships. Li and Dafalias [6] proposed a simple approach which accounts for the effect of the relative orientation of the stress and fabric tensors. This is done by the proper definition of a scalar-valued state variable A which is a function of both F_{ij} and σ_{ij}.

The tensor T_{ij} which is a function of both the fabric and stress tensors is defined as follows [6, 22]:

$$T_{ij} = \frac{1}{6}\left(\sigma_{im}\, F^{-1}_{mj} + F^{-1}_{in}\, \sigma_{nj}\right) \tag{39}$$

where F^{-1}_{in} is inverse of the fabric tensor F_{in}.

T_{ij} reflects the influence of the material fabric and its relative orientation with respect to stress. It is affected by the magnitude of the stress. Thus it is not suitable for direct use in describing the anisotropic stress states of a material. For example if a material is isotropic (i.e. $T_{ij} = \sigma_{ij}$), a scalar-valued index derived from T_{ij} changes with the magnitude of σ_{ij} instead of having a unique value which is characteristics of the isotropic state. Hence some sorts of normalization relative to stress seem to be necessary [6].

We start with decomposition of the stress tensor into a deviatoric stress tensor and a hydrostatic stress tensor as follows:

$$\sigma_{ij} = s_{ij} + p\delta_{ij} = p(\eta_{ij} + \delta_{ij}) \tag{40}$$

where δ_{ij} is Kronecker delta.

Stress ratio R_f and the load angle θ are defined based on η_{ij} as follows [6]:

$$R_f = \sqrt{\frac{3}{2}\eta_{ij}\eta_{ij}} \tag{41}$$

$$\theta = -\frac{1}{3}\sin^{-1}\left(\frac{9}{2}\frac{\eta_{ij}\eta_{jk}\eta_{ki}}{R_f^3}\right) \tag{42}$$

A critical state failure surface in stress space is defined using R_f and θ as [6]:

$$R_f - M_c g(\theta) = 0 \tag{43}$$

where M_c is the critical stress ratio under triaxial compression, and

$$g(\theta) = \frac{\sqrt{(1+c^2)^2 + 4c(1-c^2)\sin 3\theta} - (1+c^2)}{2(1-c)\sin 3\theta} \tag{44}$$

Which is an interpolation function that interpolates R_f on the critical state failure surface based on θ such that $g(-30) = 1$, $g(0) = (c+c^2)/(1+c^2)$, and $g(30) = c$. c is a model constant which defines the ratio of the critical state ratio under triaxial extenstion over that of triaxial compression. Not all values of c result in $g(-30) = 1$ and $g(30) = c$. For example $c \leq 0.41$ does not lead to $g(-30) = 1$. However all typical values of c (say $0.6 < c < 1$) satisfy the above conditions.

Note that the critical state failure surface defined by equation (43) is independent of the material anisotropy. This is justified by the fact that the critical stress ratio is mainly controlled by the frictional coefficient between sand particles which is an intristic property and independent of the fabric [6].

As mentioned the effect of the fabric anisotropy must only deponds on the orientation, and not the magnitude of the stress tensor. A stress $\hat{\sigma}_{ij}$ normalized with respect to mean effective stress and with deviatoric directions identical to those of σ_{ij}can be defined as follows [6]:

$$\hat{\sigma}_{ij} = \left(\sqrt{\frac{2}{3}} M_c g(\theta)\right) l_{ij} + \delta_{ij} = \hat{\eta}_{ij} + \delta_{ij} \tag{45}$$

where

$$l_{ij} = \frac{\eta_{ij}}{|\eta_{mn}|} = \sqrt{\frac{3}{2}} \frac{\eta_{ij}}{R_f} \tag{46}$$

is a unit tensor which represents the direction of the stress ratio tensor η_{ij}.

$\hat{\sigma}_{ij}$ clearly includes information on the stress orientation by l_{ij}. If we use $\hat{\sigma}_{ij}$ instead of σ_{ij} in equation (39), a normalized stress tensor can be defined as follows [6]:

$$\tilde{T}_{ij} = \frac{1}{6}\left(\hat{\sigma}_{im} F_{mj}^{-1} + F_{in}^{-1} \hat{\sigma}_{nj}\right) \tag{47}$$

$\tilde{T}_{ij}$ can be decomposed into a deviatoric stress ratio tensor $\tilde{\eta}_{ij}$ and a hydrostatic part $\tilde{p} = \tilde{T}_{jj}/3$, as follows:

$$\tilde{T}_{ij} = \tilde{p}\left(\tilde{\eta}_{ij} + \delta_{ij}\right) \tag{48}$$

Similar to equations (41) and (42), $\tilde{R}_f$ and $\tilde{\theta}$ are defined as follows [6]:

$$\tilde{R}_f = \sqrt{\frac{3}{2}\tilde{\eta}_{ij}\tilde{\eta}_{ij}} \tag{49}$$

$$\tilde{\theta} = -\frac{1}{3}\sin^{-1}\left(\frac{9}{2}\frac{\tilde{\eta}_{ij}\tilde{\eta}_{jk}\tilde{\eta}_{ki}}{\tilde{R}_f^3}\right) \tag{50}$$

After some calculations, $\tilde{\eta}_{ij}$ and $\tilde{R}_f$ can be expressed in terms of $\hat{\sigma}_{ij}$ and F_{ij}^{-1} as follows [6]:

$$\underline{\tilde{\eta}} = \frac{3}{2} tr^{-1}\left(\underline{\hat{\sigma}}\,\underline{F}^{-1}\right)\left(\underline{\hat{\sigma}}\,\underline{F}^{-1} + \underline{F}^{-1}\underline{\hat{\sigma}}\right) - I \tag{51}$$

$$\tilde{R}_f = \sqrt{\frac{27}{4} tr^{-2}\left(\underline{\hat{\sigma}}\,\underline{F}^{-1}\right)\left(tr\left(\underline{\hat{\sigma}}^2\underline{F}^{-2}\right) + tr\left(\underline{\hat{\sigma}}\,\underline{F}^{-1}\underline{\hat{\sigma}}\,\underline{F}^{-1}\right)\right) - \frac{9}{2}} \tag{52}$$

The symbol tr denotes the trace of a tensor, and underbar sign indicates a tensorial quantity.

Anisotropic state parameter A is ultimately defined as a function of $\tilde{R}_f$ and $\tilde{\theta}$ using equation (43) as follows:

$$A = \frac{\tilde{R}_f}{M_c g(\tilde{\theta})} - 1 \tag{53}$$

Parameter A can be used as a parameter for describing the sand fabric effect on constitutive behaviour. It can be shown that for isotropic material $A = 0$ while for anisotropic materials it can be either positive or negative, depending on the orientation of the stress relative to that of the soil fabric and to a weaker degree on the fabric intensity [6].

Changes of anisotropic parameter A with α and b is shown in Fig. 2 for chosen values of $\Delta = 0.2$, $M_c = 1.25$, and $c = 0.75$. α is the angle between the direction of the major principal stress and direction of deposition (usually vertical direction). b is b-parameter which is used to investigate effect of the intermdiate principal stress and is defined as follows:

$$b = \frac{\sigma_2 - \sigma_3}{\sigma_1 - \sigma_3} \tag{54}$$

Triaxial compression (TC) and triaxial extension (TE) are two extreme modes of shearing which are associated with $b = 0,\ \alpha = 0$ and $b = 1,\ \alpha = 90$ respectively. The hollow cylinder (HC) test can provide tests with constant $0 < \alpha < 90$ and constant $0 < b < 1$ which are other modes of shearing between two extreme modes of TC and TE. The HC apparatus permits independent control on the magnitutde and direction of the three principal stresses (i.e. rotation of the major-minor principal stress axes). Thus HC apparatus can be used for studies of inherent anisotropy, intermediate principal stress, and rotation of major/minor principal stress direction [23].

A schematic representation of the HC apparatus is shown in Fig. 3. During HC tests, the axis of σ_1 and σ_3 rotate by α around the fixed axis of $\sigma_2 = \sigma_{rr}$. This means one direction always remains principal direction during HC tests. Also directions of σ_{zz}, σ_{rr}, and $\sigma_{\theta\theta}$ correspond to those of F'_{11}, F'_{22}, and F'_{33} in equation (38). Any HC element is subjected to an axial load, F_v, torque, T, internal pressure, p_i, and external pressure, p_o. During shearing, the torque T develops shear stresses, $\tau_{\theta z}$ and $\tau_{z\theta}$ which are equal. The axial load causes a vertical stress, σ_{zz}, and p_i and p_o determine σ_{rr} and $\sigma_{\theta\theta}$ [6, 9, 23]. During HC test, there may or may not be pressure

applied in the inner hole. If the inner pressure is zero, the inner wall will fail under the confining stresses. However spalling will continue around the inner wall until the arching develops. Arching will reduce the stress on the wall until it is low enough leading to instability of inner wall.

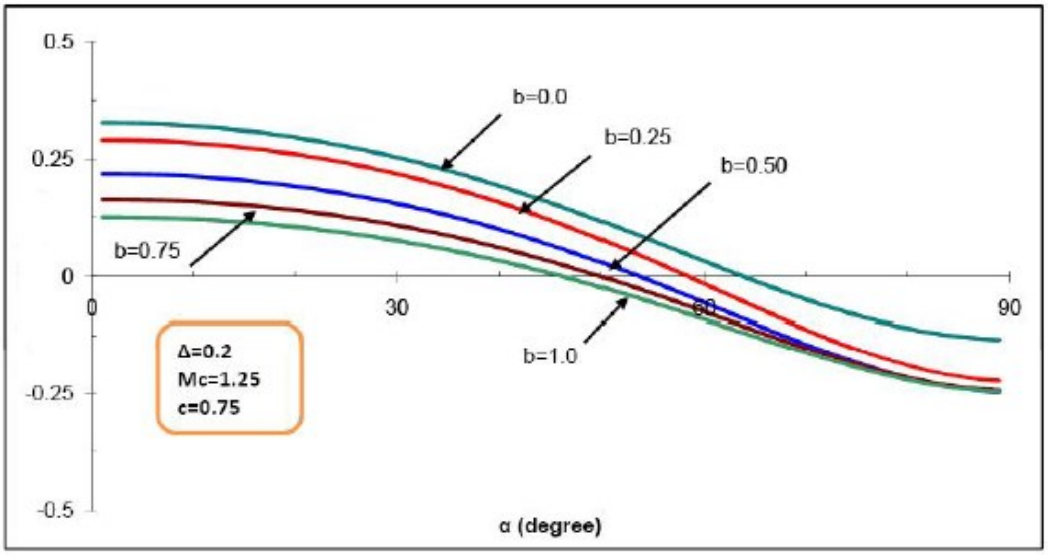

Fig. 2 Changes of anisotropic state parameter *A* (vertical axis) with *α* and *b* [22]

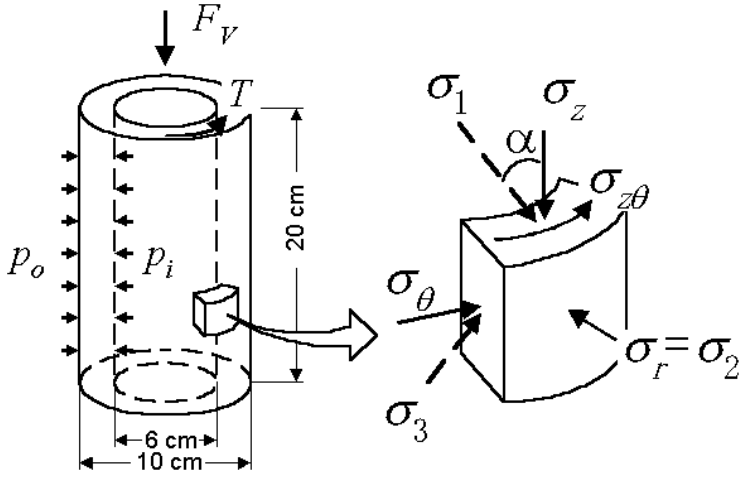

Fig. 3 Schematic representation of hollow cylinder apparatus [24]

5. Modification of the proposed constitutive model using anisotropic state variable

Incorporation of anisotropic parameter A into the constitutive model is done similar to Rasouli [22]. He incorporated A by modifying the definition of M_p in the constitutive equations. Some important features of the model such as the plastic modulus, the yielding stresses, and consequently the stress-dilatancy relationship are affected by this stress ratio because the loading function includes M_p. These features will be a function of anisotropic state parameter if M_p is made a function of A. However, other features of the model like the failure stress ratio and critical state are not influenced by M_p. Thus, they are considered to remain unchanged by inherent anisotropy as in Manzari and Dafalias [18].

Definition of M_p intially is modified in order to include b-parameter for different modes of shearing as follows [9, 25]:

$$M_p = \frac{6(1 - b + b^2)^{1/2} sin\varphi_p}{3 + (2b - 1) sin\varphi_p} \tag{55}$$

For $b = 0$ and $b = 1$, the formula will reduce to those of $M_{p,c}$ and $M_{p,e}$, respectively, in which subscript c stands for compression and subscript e denotes extension.

In order to account for the effects of inherent anisotropy and all modes of shearing including triaxial compression and triaxial extension, $sin\varphi_p$ is defined using the following formula [22]:

$$\sin \varphi_p = \sin \varphi_\mu - k_p \psi_p - a_p(A) \tag{56}$$

in which

$$a_p(A) = \frac{A_c - A}{A_c - A_e} . a_p \tag{57}$$

where A_c and A_e are the anisotropic parameters in triaxial compression and triaxial extension, respectively, whose values depend on other inherent anisotropy related model parameters including Δ, c, and M_c. A_c and A_e can be located in Fig. 2 as far upper left side and far lower right side, respectively. A_c corresponds to $b = 0$ and $\alpha = 0$, while A_e corresponds to $b = 1$ and $\alpha = 90$. For triaxial compression $A = A_c$ and $a_p(A) = 0$, and for triaxial extension $A = A_e$ and $a_p(A) = a_p$.

It should be noted that in this model, it is assumed that elastoplastic behavior takes place as soon as loading commences in stress space. This is in accordance with experimental observations which suggest that truly elastic behaviour of sand occurs at very low values of shear strain [4, 26]. Therefore, fabric anisotropy in this model is incorporated for elastoplastic response.

6. Model performance

Performance of the proposed model is examined against hollow cylinder tests on Toyoura sand. These tests have been conducted under different values of α and b. All specimens in these undrained tests were consolidated isotropically to $100\ kPa$ before being sheared. They come from Rasouli [22]. However they originally come from Yoshimine et. al. [24]. Note that some combinations of α and b were not tested during these HC tests because of uncontrolled non-uniformities and instabilities. In general, conducting HC tests with high values of b (say $b \geq 0.75$) is difficult since it is difficult to perform such tests due to non-uniformity of straining developed during these tests [22].

The angle α changes in HC tests with change of the major principal stress relative to the vertical direction which is the deposition direction. However, it is assumed here that it varies with change of the deposition direction (which is perpendicular to the bedding plane) relative to the vertical direction which is direction of the major principal stress. Axisymmetric mode is also used in order to resemble a cylindrical sample.

All of the following tests on Toyoura sand were modelled by one unique set of model parameters which are listed in table 1. Inherent anisotropy parameters were selected according to Li and Dafalias [6]. Assigned values for Δ, c and M_c result in $A_c = 0.328$ and $A_e = -0.25$. Note that Δ, c and M_c are used to estimate a value for A under different combinations of α and b.

Measured and predicted behaviour of Toyoura sand under undrained HC tests with different values of α and b are shown in Figs. 4 to 13. They are in relatively good agreement in general even though there are discrepancies in some cases. It was possible to capture better matches for those cases if a

non-unique set of model parameters were used. However, the aim was to capture the experimental observations using one single set of model parameters. This aim resulted in similar inaccuracies in calibration of the HC tests in Rasouli [22] too. Note that the reduced extension test was modelled for the test with $b = 1$ rather than the standard extension test (i.e. decreasing axial strain/stress was modelled). A zero value was assigned for all bonding related parameters in these simulations.

Table 1 Material parameters used for calibration of undrained HC tests on Toyoura sand

Parameter type	Name	Toyoura sand
Peak state	k_p φ_μ a_p	1.2 21 0.45
Stress-dilatancy	φ_{cs} k_{PT} a_{PT}	31 0.75 0.01
Elasticity	G_a K_a	8e6 8.5e6
Plastic stiffness	h	1
Failure	k_f	0.75
Critical state line	e_{cs}	$-0.0063477p^3 + 0.0367p^2$ $- 0.11991p + 0.92548$ $(p\ in\ MPa)$
Inherent anisotropy	Δ M_c c	0.2 1.25 0.75

Fig. 4, 6 and 10 reveals that sand resistant against liquefaction decreases with an increase in value of α at a given value of b. Test with $\alpha = 0$ in Fig. 4 shows that the sand sample has experienced clear strain hardening with an obvious phase transformation shown in Fig. 5. That is, initially positive pore pressure develops within sample which results in continuous decrement in the mean effective stress value. However when the stress path reaches the maximum contraction capacity (i.e. phase transformation surface), the material undergoes dilation and consequently negative pore pressure develops which leads to an increasing trend in the mean effective stress and hence the material strengthening. Test with

$\alpha = 15$ reflects similar behavior, but with less stiff response. Test with $\alpha = 30$ shows less stiff response compared to the aforementioned tests. It also reveals that short softening response (i.e. the material weakening) is accompanied by hardening response (i.e. the material strengthening). The strongest softening behavior has taken place in test with $\alpha = 45$ accompanied by the phase transformation and hardening. Similar behaviors are observed in other tests (Fig. 6-13). Note that full liquefaction has occurred in some tests when the stress path has approached the origin of the coordinate system (Figs. 7 and 13).

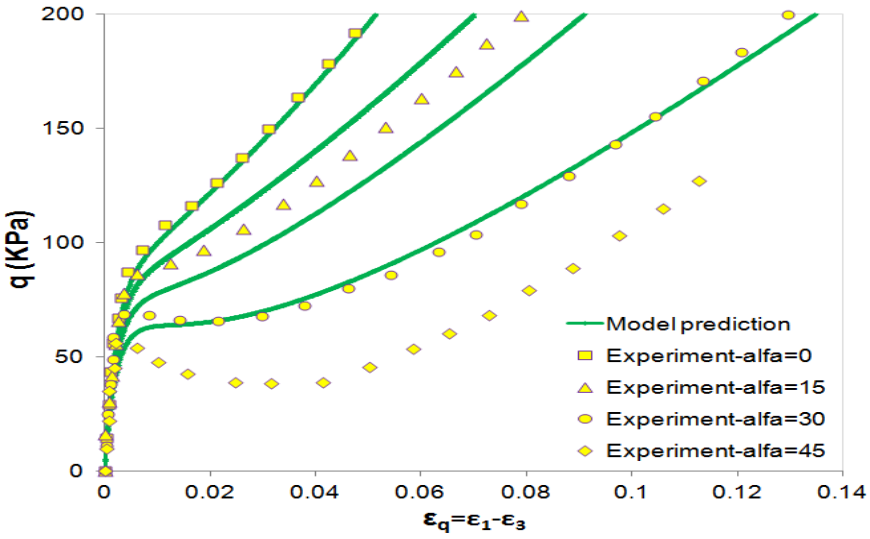

Fig. 4 Observed and predicted undrained response for deviator stress vs. shear strain curve under $b = 0$ and $\alpha = 0^0$ *to* 45^0

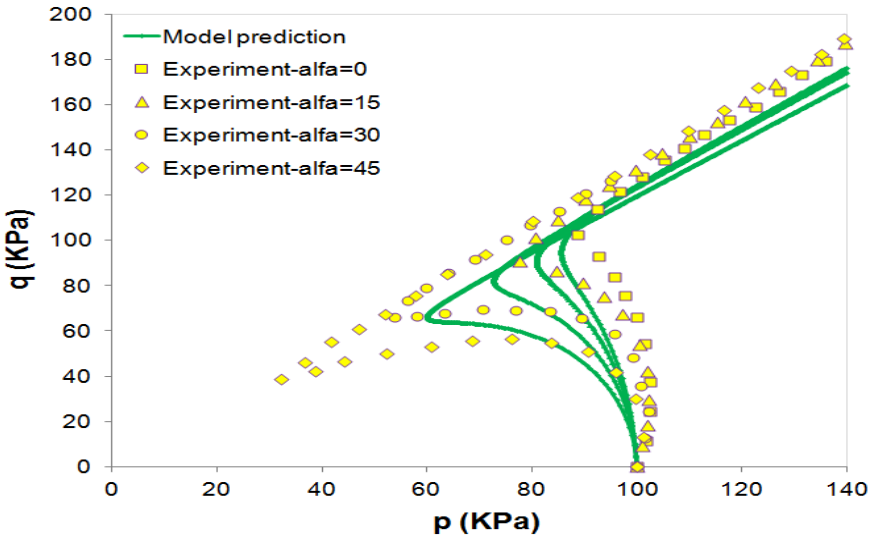

Fig. 5 Observed and predicted undrained response for deviator stress vs. mean effective stress curve under $b = 0$ and $\alpha = 0^0$ to 45^0

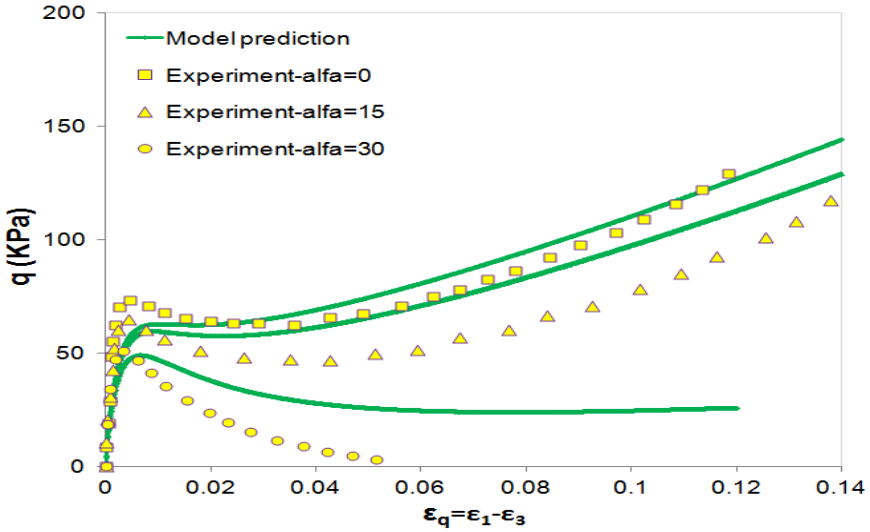

Fig. 6 Observed and predicted undrained response for deviator stress vs. shear strain curve under $b = 0.25$ and $\alpha = 0^0$ to 30^0

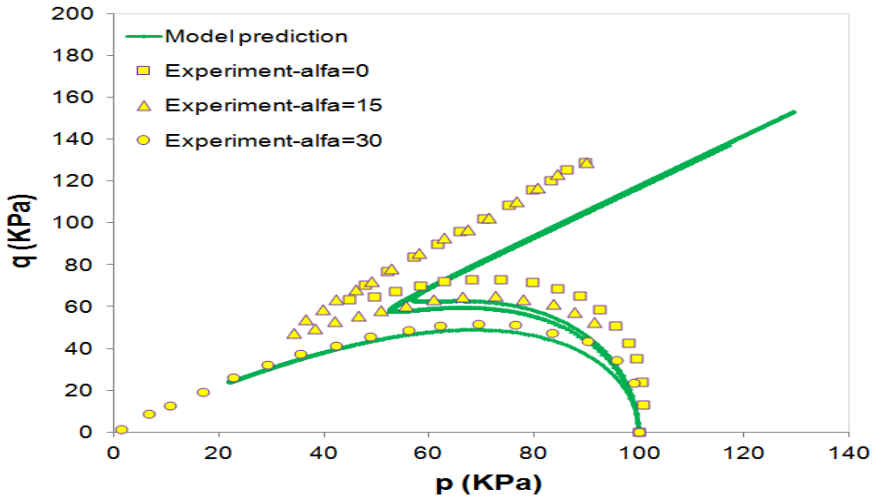

Fig. 7 Observed and predicted undrained response for deviator stress vs. mean effective stress curve under $b = 0.25$ and $\alpha = 0^0$ to 30^0

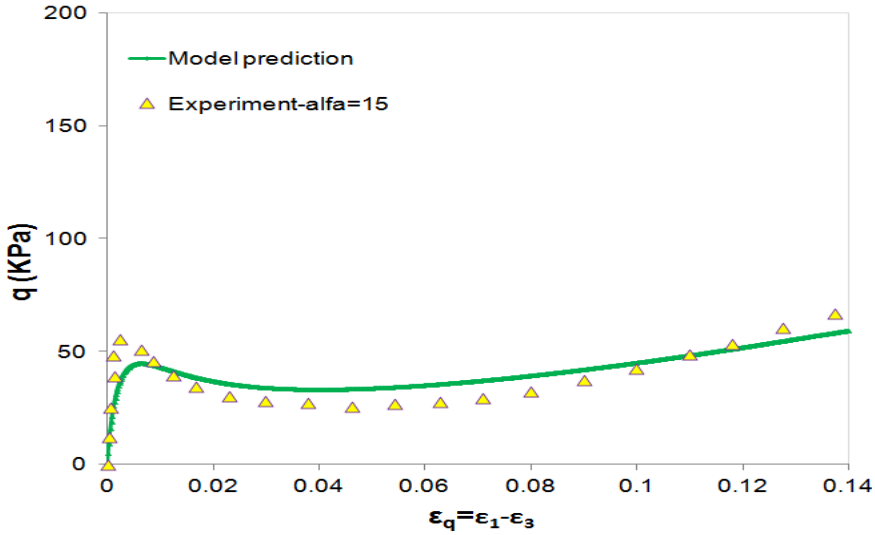

Fig. 8 Observed and predicted undrained response for deviator stress vs. shear strain curve under $b = 0.5$ and $\alpha = 15^0$

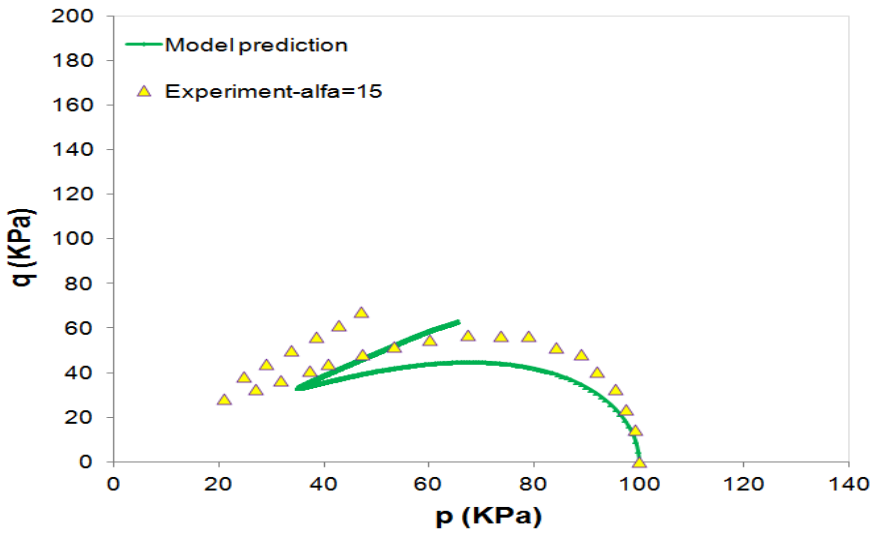

Fig. 9 Observed and predicted undrained response for deviator stress vs. mean effective stress curve under $b = 0.5$ and $\alpha = 15^0$

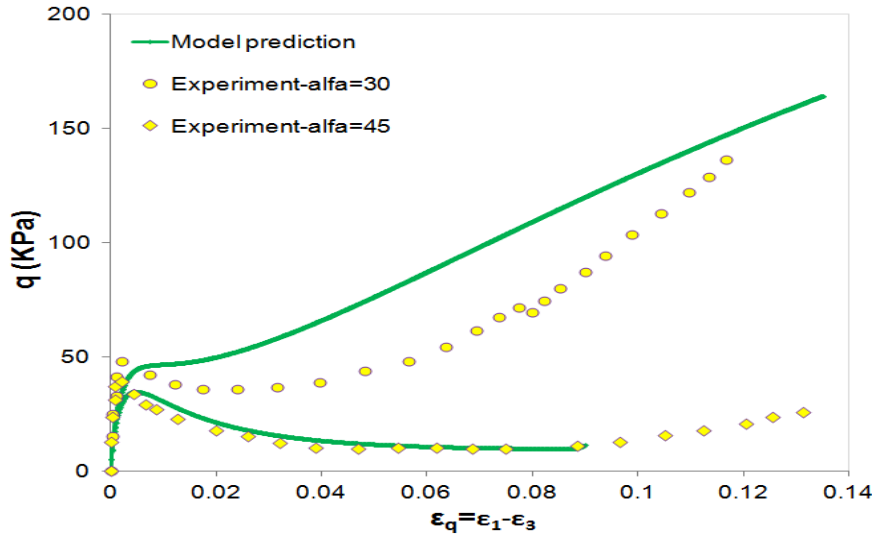

Fig. 10 Observed and predicted undrained response for deviator stress vs. shear strain curve under $b = 0.75$ and $\alpha = 30^0$ *to* 45^0

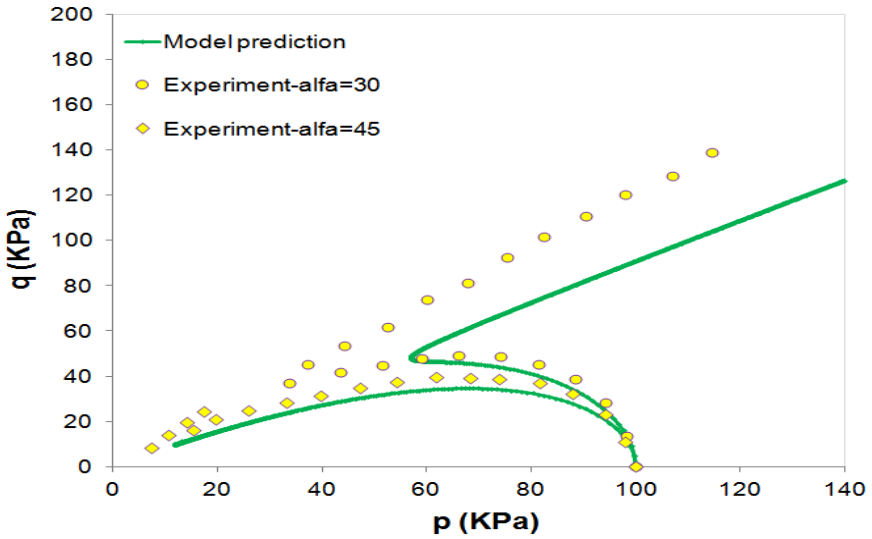

Fig. 11 Observed and predicted undrained response for deviator stress vs. mean effective stress curve under $b = 0.75$ and $\alpha = 30^0$ *to* 45^0

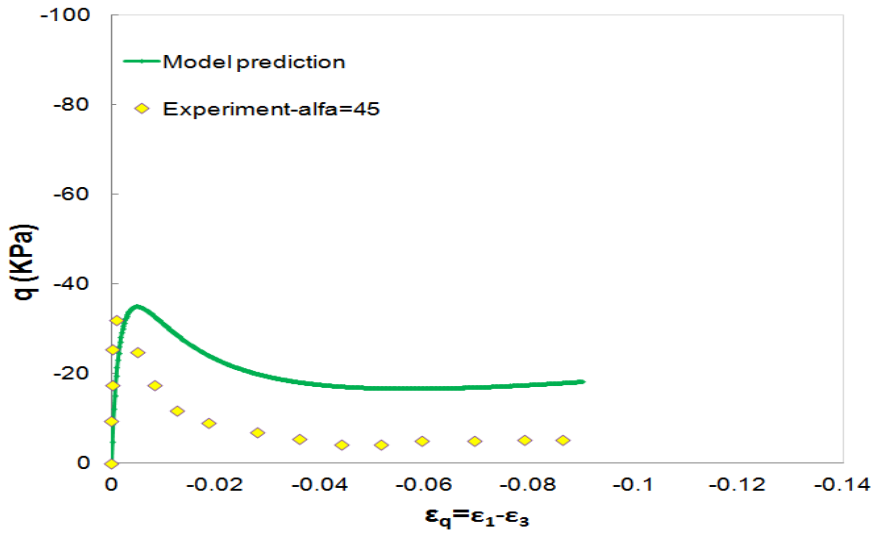

Fig. 12 Observed and predicted undrained response for deviator stress vs. shear strain curve under $b = 1.0$ and $\alpha = 45^0$

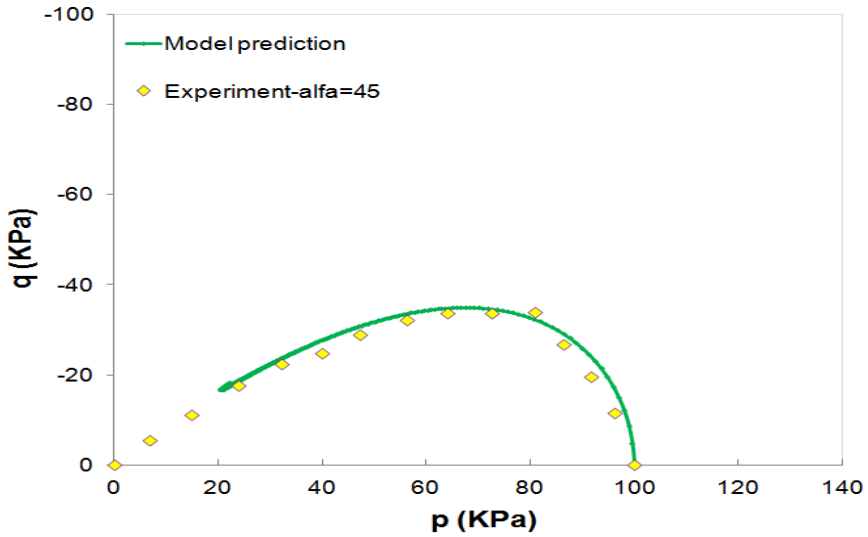

Fig. 13 Observed and predicted undrained response for deviator stress vs. mean effective stress curve under $b = 1.0$ and $\alpha = 45^0$

Figs. 14 and 15 show model predictions for drained HC tests on a hypothetical cemented sand. These tests have been modelled using one set of model parameters which are listed in table 2. Intrinsic anisotropy parameters were chosen similar to those in table 1. It was assumed also that all speciments were consolidated isotropically to pressure equals to 200 kPa and void ratio equals to 0.74 before being sheared.

Table 2 Material parameters used for calibration of hypothetical drained HC tests on cemented sand in Figs. 14 to 15

Parameter type	Parameter name	Cemented sand
Original model	k_p	1.5
	φ_μ	29
	a_p	0.15
	φ_{cs}	31
	k_{PT}	1.25
	a_{PT}	0.10
	G_a	5e6
	K_a	8e6
	h	1
	k_f	0.75
	e_{cs}	$-0.0063477p^3 + 0.0367p^2 - 0.11991p + 0.76$ (p in MPa)
Bonding (cementation)	p_o	2e5
	γ	15
	β	0.1
	c	5e3
	ξ	5

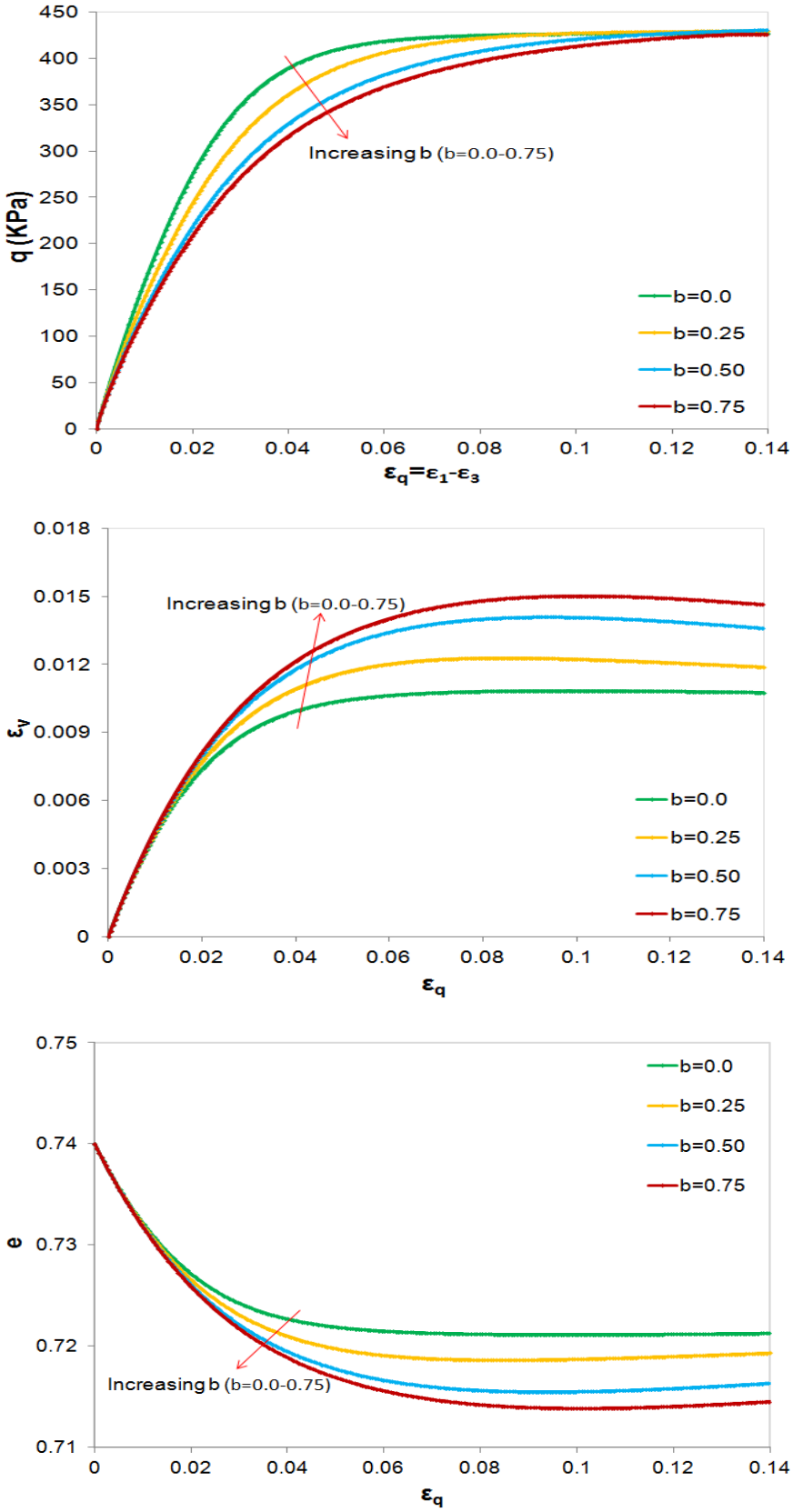

Fig. 14 Sensitivity analysis for a cemented sand under HC tests with $\alpha = 0^0$

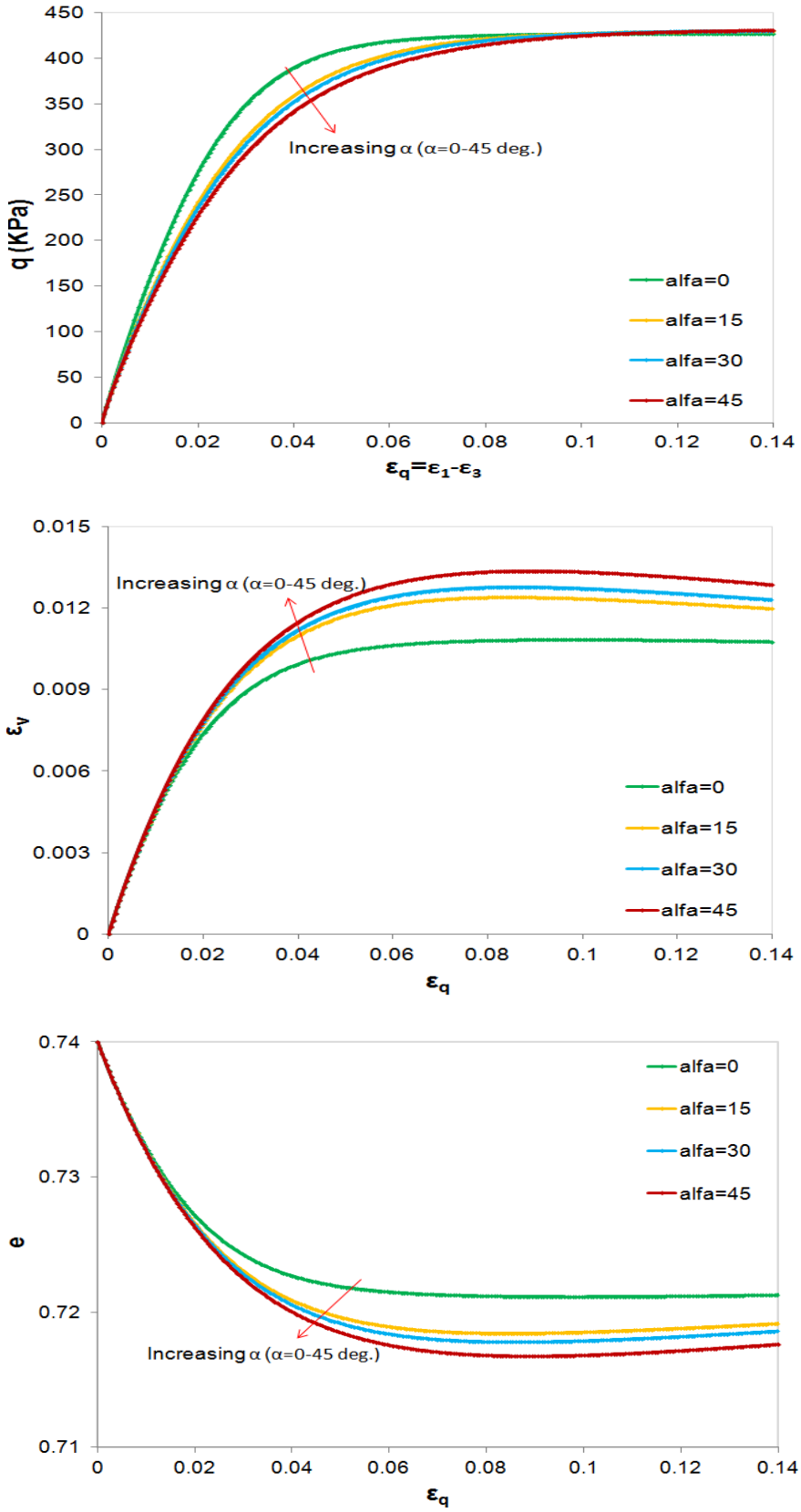

Fig. 15 Sensitivity analysis for a cemented sand under HC tests with $b = 0.25$

Results of sensitivity analysis in Fig. 14 reveal that the stiffness of cemented sand decreases with increasing the value of b, implying that TC and TE have the greatest and the lowest stiffness, respectively. Unlike stiffness, the tendency for contraction increases with increasing value of b which means TC and TE have respectively the lowest and the highest tendency for contraction under a given initial and boundary conditions. This implies that the greater positive pore pressure will develop under undrained conditions for higher values of b leading to smaller resistant against liquefaction. These interpretations suggest that TC and TE, two extreme modes of shearing, are the strongest and the weakest modes of shearing, correspondingly, for identical conditions. This is in line with the literature [2, 3, 6, 9].

Sensitivity analysis results in Fig. 15 show that the stiffness of weakly cemented sand in a given value of b decreases with increasing the value of α. Unlike stiffness, the tendency for contraction increases with increasing value of α. This implies that the greater positive pore pressure will develop under undrained conditions for higher values of α which result in smaller resistant against liquefaction. This is in accordance with the literature [3, 20]. That is, most contact normals are oriented in the vertical direction when the bedding plane is horizontal (i.e. deposition direction is vertical) which causes the specimen to be strong. However when the bedding plane is vertical (i.e. deposition direction is horizontal), most contact normals are oriented horizontally which causes the specimen to be weak in vertical direction [2, 20].

Figs. 16 and 17 show model predictions for hypothetical cyclic HC tests on the same weakly cemented sand. In addition to model parameters listed in Table 2, cyclic loading related model parameters were chosen in this sensitivity analysis as follows:

$c_1 = 5e6, c_2 = 500, R_u = 3$

It was also assumed that the speciments were consolidated isotropically to pressure equals to $200\ kPa$ and void ratio equals to 0.74 before being sheared similar to monotonic HC tests on the same weakly cemented sand.

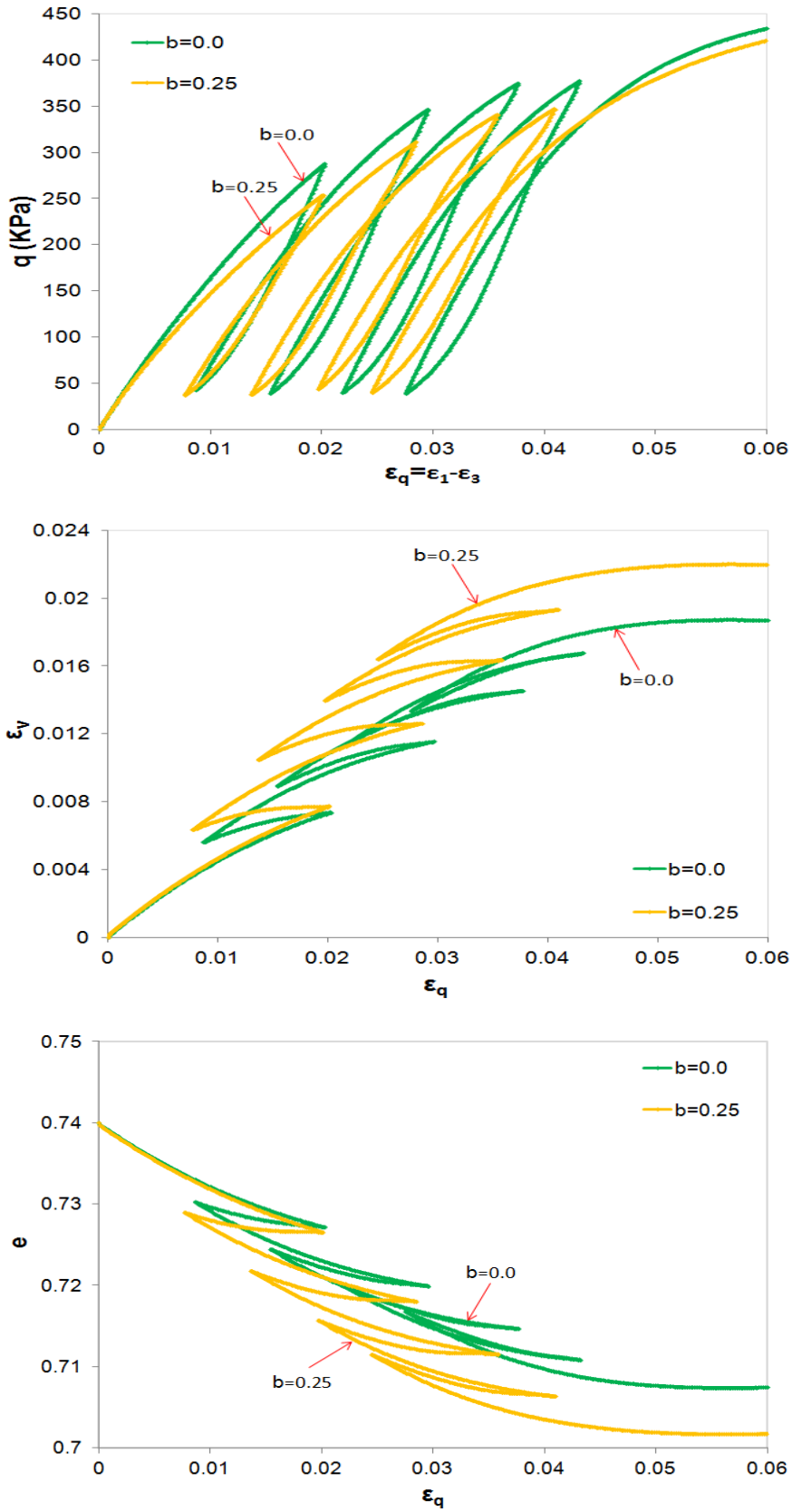

Fig. 16 Sensitivity analysis for cyclic HC tests with $\alpha = 0$ and $b = 0$ & 0.25

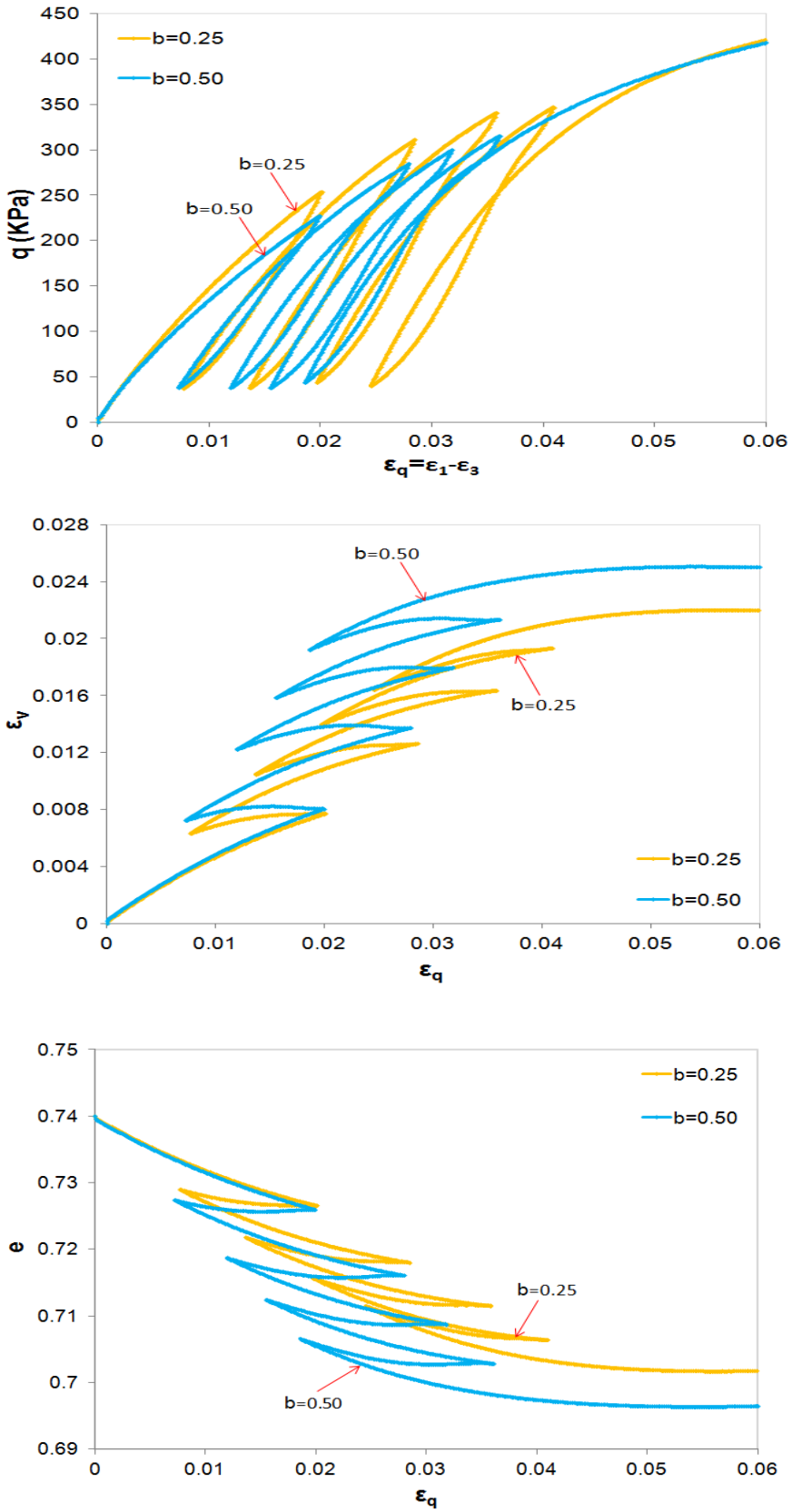

Fig. 17 Sensitivity analysis for cyclic HC tests with $\alpha = 0$ and $b = 0.25$ & 0.5

Fig. 18 shows cohesion degradation during hypothetical cyclic HC test with $b = 0$ in Fig. 16. About 50% of total degradation (i.e. about 2000 Pa) occurs during cycle of unloading-reloading. This means if conventional plasticity is used, cohesion degradation will be underestimated by about 50% since no plastic deformation is calculated by classical plasticity during cycle of unloading-reloading. Cohesion degradation during unloading-reloading cycle depends profoundly on unloading plastic modulus in the proposed constitutive model. Thus for other cases where $R_u > 3$, say $R_u = 15$, contribution of unloading-reloading cycles in total cohesion degradation is significantly much smaller than this case. However even small cohesion degradation during unloading-reloading will affect predicted outcomes because it will accumulate during successive cycles. Therefore it is required to record plastic deformation for stress paths inside the yield surface during cycles of unloading-reloading.

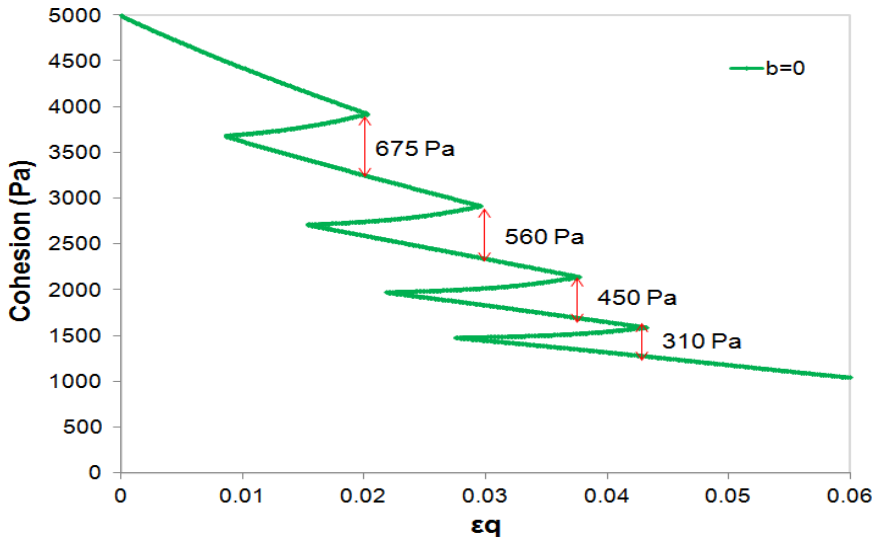

Fig. 18 Cohesion degradation during cyclic HC test with $\alpha = 0$ and $b = 0$

7. Conclusion

The overall response of sand depends not only on the cementation bonds between sand particles, but also on intermediate principal stress and fabric which reflect particle orientation and particle contact arrangements. Therefore, the fabric and intermediate principal stress as influential parameters should be incorporated into constitutive model in order to accurately capture mechanical behavior of

sand/cemented sand under various shearing/deformation conditions. Thus fabric was incorporated into the model using a fabric tensor which represents material inherent anisotropy and a scalar-valued state variable which describes the material anisotropic state. To account for intermediate principal stress effect, b-parameter was also integrated into formulation of the model. Performance of the unparallelled proposed constitutive model was examined against HC monotonic tests on Toyoura sand. Model predictions are in reasonable agreements with experimental observations. The model was also used to predict behavior of a weakly cemented sand under cyclic HC tests with different values of b and α. Model predictions show that stiffness of cemented sand decreases and tendency for contraction increases with increasing values of b under a given α or with increasing values of α under a given value of b. These observations suggest that TC $(b = 0, \alpha = 0)$ and TE $(b = 1, \alpha = 90)$, two extreme modes of shearing, are the strongest and the weakest modes of shearing, respectively.

Simulated outcomes suggest also that inaccurate results will produce if plastic deformation is neglected during cycle of unloading-reloading. Hence use of an advanced plasticity theory such as bounding surface plasticity is required in order to capture cyclic response of sand/cemented sand more accurately.

Acknowledgement

The authors would like to acknowledge the research funding for this study provided by NSERC through a Collaborative Research Development program supported by BP Canada.

References

[1] Wan RG, Guo, PJ. Drained cyclic behavior of sand with fabric dependence. Journal of Engineering Mechanics 2001a; 127(11): 1106-1116.

[2] Wan RG, Guo PJ. Stress dilatancy and fabric dependencies on sand behavior. Journal of Engineering Mechanics 2004; 130(6): 635-645.

[3] Gao Z, Zhao J. Constitutive modeling of artificially cemented sand by considering fabric anisotropy. Computers and Geotechnics 2012; 41: 57-69.

[4] Jefferies MG. Nor-Sand: a simple critical state model for sand. Géotechnique 1993; 43(1): 91-103.

[5] Li, XS. Calibration of an anisotropic sand model. In Proceedings from GeoFrontiers: Calibration of Constitutive Models, ASCE, Austin; 2005. p. 1-12.

[6] Li XS, Dafalias YF. Constitutive modeling of inherently anisotropic sand behaviour. Journal of Geotechnical and GeoEnvironmental Engineering 2002; 128 (10): 868-880.

[7] Reilly MPO, Brown SF. Cyclic loading of soils: from theory to design. Blackie and son limited, UK; 1991.

[8] Armstrong PJ, Frederick CO. A mathematical representation of the multiaxial Bauschinger effect. CEGB Report, RD/B/N731, Berkeley Nuclear Laboratories; 1966.

[9] Imam MR. Modeling the constitutive behavior of sand for the analysis of static liquefaction. Ph.D. thesis, The University of Alberta, Edmonton, Canada; 1999.

[10] Imam MR. Morgenstern NR, Robertson PK, Chan, DH. A critical state constitutive model for liquefiable sand. Canadian Geotechnical Journal 2005; 42(3): 830-855.

[11] Yu HS, Tan SM, Schnaid F. A critical state framework for modeling bonded geomaterials. Geomechanics and Geoengineering 2007; 2(1): 61-74.

[12] Been K, Jefferies MG. A state parameter for sands. Geotechnique 1985; 35(2): 99-112.

[13] Yin ZY, Chang CS. Stress-dilatancy behavior for sand under loading and unloading conditions. International Journal for Numerical and Analytical Methods in Geomechanics. 2013; 37(8): 855-870

[14] Rowe PW, The stress–dilatancy relations for static equilibrium of an assembly of particles in contact. Proceedings of the Royal Society of London Series A; 1962. p.500–527.

[15] Roscoe KH, Schofield AN, Thurairajah A. Yielding of clays in states wetter than critical. Geotechnique 1963;13(3): 211–240.

[16] Nova RA. Constitutive model for soil under monotonic and cyclic loading. In Soil mechanics transient and cyclic loads, Pande GN, Zienkiewicz OC. Wiley: Chichester 1982; p. 343–373.

[17] Jefferies MG. Plastic work and isotropic softening in unloading, Geotechnique 1997; 47(5):1037–1042.

[18] Manzari MT, Dafalias YF. A critical state two-surface plasticity model for sands. Geotechnique 1997; 47(2):255–272.

[19] Gajo A, Wood D. Severn-Trent sand: a kinematic hardening constitutive model: the q-p formulation. International Journal for Numerical and Analytical Methods in Geomechanics 1999; 23(9):925–965.

[20] Wan RG, Guo PJ. Effect of microstructure on undrained behaviour of sands. Canadian Geotechnical Journal 2001b; 38(1):16-28.

[21] Oda M, Nakayama H. Yield function for soil with anisotropic fabric. Journal of Engineering Mechanics 1989; 115(1): 89-104.

[22] Rasouli R. Modelling of anisotropic behavior of sands. M.Sc. thesis, AmirKabir University of technology, Tehran, Iran; 2010.

[23] Cai Y. An experimental study of non-coaxial soil behaviour using hollow cylinder testing. Ph.D. thesis, The University of Nottingham, Nottingham, U.K; 2010.

[24] Yoshimine M, Ishihara K, Vargas W. Effects of principal stress direction and intermediate principal stress on undrained shear behaviour of sand. Soils and Foundations 1998; 38(3):179–188.

[25] Imam MR, Rasouli, R. Introduction of inherent anisotropy into a critical-state constitutive model for sands, proceedings of the 63td Canadian Geotechnical Conference, Calgary, Canada; 2010. p.168-175.

[26] Khong, CD. Development and numerical evaluation of unified critical state models. PhD thesis, The University of Nottingham, Nottingham, U.K; 2004.